Membrane and Water Treatment, *Vol. 17, No. 3 (2026) 239-258*
https://doi.org/10.12989/mwt.2026.17.3.239

Techno-Press

Experimental study and parametric effects for breaking of butyric acid/water azeotrope using air gap membrane distillation

Rajeshwar K. Kholapure, Kailash Singh*, Sushant Upadhyaya

Department of Chemical Engineering, Malaviya National Institute of Technology, Jaipur, Rajasthan 302017, India

(Received July 23, 2025, Revised April 11, 2026, Accepted April 16, 2026)

Abstract. In this work, the feasibility of air gap membrane distillation for breaking the butyric acid/water azeotrope is examined. The azeotropic mixture was passed through the set up equipped with a porous, hydrophobic PTFE membrane. The effect of various process variables, including feed temperature, feed flow rate, coolant temperature, coolant flow rate, and air gap width on total permeate flux, selectivity of butyric acid, and permeate and retentate concentration has been studied. Furthermore, EDS and FE-SEM were used to investigate how operating time impacts morphology of membrane. The SEM image of membrane was analysed with ImageJ software to determine the pore size distribution. The experimental findings indicate that the total flux increases from 0.54 to 9.81 kg/m^2·h on increasing the feed temperature from 40 °C to 80 °C mm at air gap width of 3mm. Total flux decreases from 2.75 to 1.01 kg/m^2·h on increasing air gap width from 3 to 11 mm at flow rate of 4 l/min. In addition, the total flux decreases from 0.54 to 0.40 kg/m^2·h when the coolant temperature is increased from 4 °C to 20 °C for air gap of 3 mm. It was observed that the butyric acid selectivity in the permeate was less than one, indicating the higher butyric acid concentration in retentate relative to permeate.

Keywords: air gap membrane distillation; butyric acid/water azeotrope; effect of process parameters; pore size distribution; PTFE hydrophobic membrane

1. Introduction

Membrane distillation (MD) technique is a non-isothermal, thermally operated separation process. In the air gap membrane distillation (ADMD) process, the hydrophobic membrane of polytetrafluoroethylene material prevents the liquid while allowing the transport of vapours. Due to the vapour pressure gradient, the vapour phase travels from the side with high vapour pressure to the side with low vapour pressure. The method involves the evaporation of feed solution on the membrane feed side, the diffusion of vapours through the pores of the membrane, air gap, and lastly condensed on a condensing plate. The temperature differential across the membrane surface generates a vapor pressure gradient, which serves as the primary driving force for mass transfer [1]. Fig. 1 depicts a schematic illustration of the various membrane distillation configurations, consisting of air gap membrane distillation (AGMD), vacuum membrane distillation (VMD), direct contact membrane distillation (DCMD), and sweep gas membrane distillation (SGMD).

*Corresponding author, Associate Professor, E-mail: ksingh.chem@mnit.ac.in

ISSN: 2005-8624 (Print), 2092-7037 (Online)

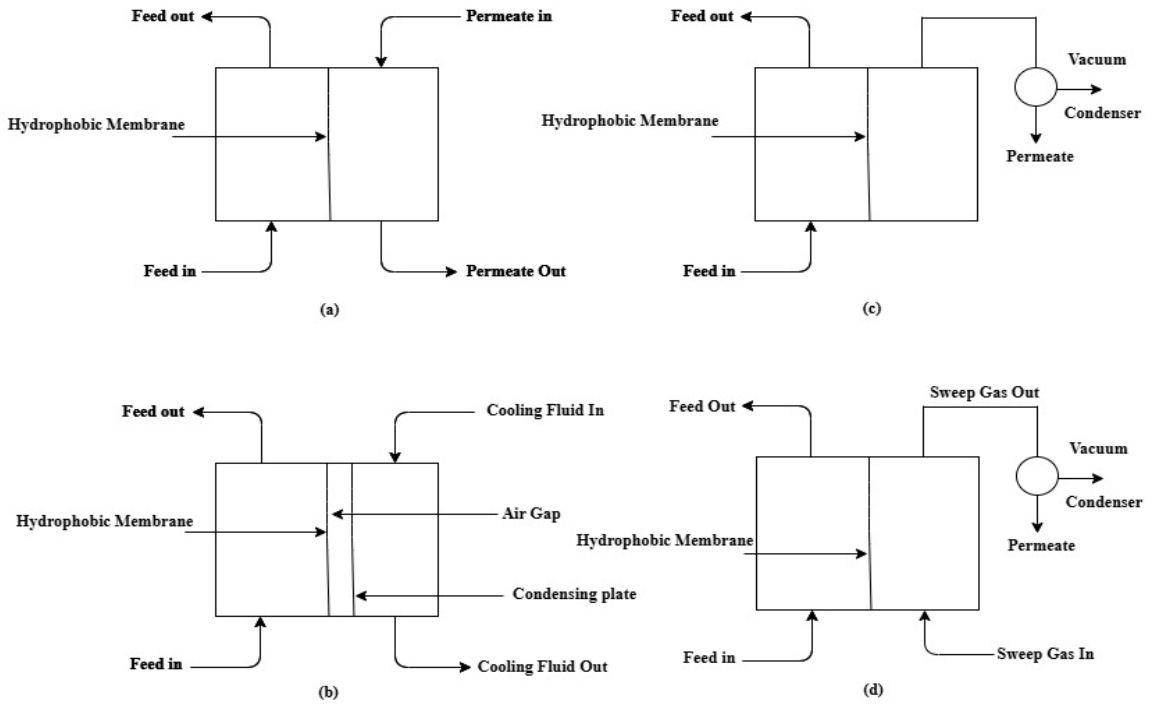

Figure 1. Techniques of membrane distillation (a) DCMD (b) AGMD (c) SGMD (d) VMD

In this study, AGMD was employed to study the breaking of butyric acid/water azeotrope. Because the relative volatility of an azeotrope is unity, separating such mixtures via conventional distillation is exceedingly difficult, as both components vaporize at a constant temperature. Various specialized techniques have been utilized to overcome azeotropic limits, including capillary distillation [2,3], adsorptive distillation [4, 5-8], diffusion distillation [9], azeotropic distillation [10-13], and extractive distillation [13-19]. While azeotropic and extractive distillation are the most common industrial methods, they possess several drawbacks, including high energy consumption, a limited selection of suitable entrainers, and inefficient recovery of the primary components [20]. Consequently, AGMD is preferred for its operational advantages in breaking azeotropic mixtures. In this process, the molecular diffusivity of the feed components through the air gap plays a crucial role; components with lower diffusivity are concentrated in the retentate, while those with higher diffusivity preferentially transport into the permeate, thereby effectively breaking the azeotrope.

Using AGMD technique, the researchers have investigated the separation of various azeotropic mixtures, including propionic acid-H_2O [21], HCl-H_2O [22-24], formic acid-H_2O [25, 26]. Udriot et al. [22] were the first to propose the use of AGMD for azeotropic separation in hydrochloric acid/water and propionic acid/water systems; they reported selectivity values of 0.60 and 0.80 for hydrochloric acid and propionic acid, respectively, at their azeotropic concentrations. The MD process is employed across a wide range of industrial applications, such as desalination of brine/sea water, the separation of volatile organic compounds (VOCs) from the organic solutions, solutions concentration, the food industry, and purification of water. Butyric acid ($CH_3CH_2CH_2COOH$) is a crucial chemical used in numerous industries, including the chemical, food, beverage, pharmaceutical,

Table 1. At one atmosphere pure components and boiling point of azeotrope for butyric acid/water azeotropic mixture

Component / azeotrope	Boiling Point of component/azeotrope (°C)	Composition of Azeotrope (weight %)
Butyric acid	165.5	-
Water	100	-
Butyric acid/water azeotrope	99.94	18.4/81.6

Table 2. Operating variables used for the experimental investigation

Process parameter	Value
Temperature of feed solution	40 - 80 °C
Flow rate of feed solution	4 - 8 l/min
Temperature of coolant	4 - 20 °C
Flow rate of coolant	4 - 8 l/min
Membrane	PTFE
Membrane thermal conductivity	0.28 W/m·K
Membrane porosity	0.85

Table 3. Membrane (PTFE) Properties

Properties	Value
Membrane material	PTFE
Membrane pore size	0.22 µm
Membrane thickness	150 µm
Membrane diameter	55 mm
Membrane porosity	85 %

polymer, paint, cosmetic, and perfume industries [27-31]. Table 1 lists the the pure boiling point of azeotrope and its individual components, while Table 2 summarize the operating variables used in this experimental investigation.

2. Materials and methods

2.1 Membrane used in the experimental study

Millipore supplied microporous hydrophobic flat-sheet polytetrafluoroethylene (PTFE) membrane used in the experiment. The physical properties and material specifications of the membrane utilised during experimentation are listed in Table 3.

2.2 Preparation of azeotropic feed solution

Certified-grade butyric acid (Loba) and laboratory-prepared distilled water were used to prepare a butyric acid/Water solution with an azeotropic feed concentration of 18.4 wt % butyric

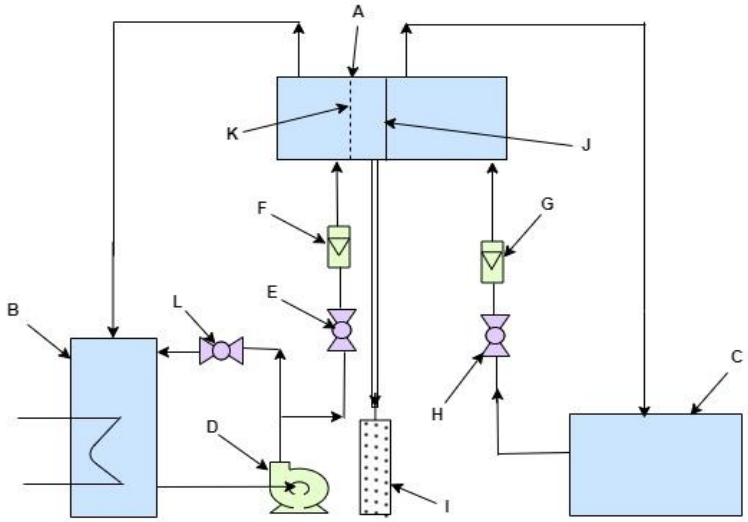

A - AGMD Module, B - Feed Tank, C - Water Chiller, D - Acid Pump, E - Feed Flow Valve,
F- Feed Flow Rotameter, G - Coolant Flow Rotameter, H - Coolant Flow Valve,
I - Permeate Receiver, J - Cooling Plate, K - Membrane, L- Bypass Valve

Figure 2. Air gap membrane distillation experimental setup

acid. The concentration of butyric acid in both the permeate and retentate was determined by the titration method. Specifically, the titration was performed using a sodium hydroxide (NaOH) solution as the titrant and phenolphthalein as the indicator.

2.3 AGMD experimental assembly

Using AGMD, the separation of Butyric acid/Water azeotropic mixtures under various operating conditions was investigated. Fig. 2 is a well-labeled diagram of the AGMD configuration employed in the experimental study. The experimental setup comprises three segments: the heated feed solution segment, the air gap or permeate segment, and the chilling segment. The microporous PTFE membrane is positioned between the heated feed solution and the air gap segment, whereas the cooling circular plate is set in between the air gap and chilling segment. Acid pump was employed to continuously circulate the heated feed solution to the feed solution segment. To achieve the target feed solution temperature, a heater was installed in the feed tank. Likewise, coolant (cold water) was continually recirculated from the water chiller to the chilling segment. Using rotameters, the flow rates of the heated feed solution and chilling water were controlled. J-Type digital thermocouples were utilised to measure heated feed solution and temperatures of coolant at entry of the AGMD module. Butyric acid and water vapours diffuse through the membrane pores and the air gap before condensing on the cooling plate. In the end, the permeate liquid was gathered in the measuring bottle.

2.4 Membrane characterization

To evaluate the morphological and structural integrity of the PTFE membranes for the separation of the butyric acid/water azeotropic mixture, several characterization techniques were employed,

as mentioned below.

2.4.1 Surface and morphological characterization

The surface and cross-sectional morphologies of the fresh and post-experimental PTFE membranes were characterized using Field Emission Scanning Electron Microscopy (FE-SEM). For the analysis, membrane specimens were first sputter-coated with a thin conductive layer of gold or carbon and subsequently mounted in a high-vacuum chamber. A field emission gun was utilized to generate a focused electron beam, scanning the membrane surface to produce high-resolution topographical and compositional micrographs. This high-resolution imaging was essential for detecting any surface fouling, pore structural changes, or evidence of pore wetting induced by the butyric acid/water mixture during the extended stability tests [32-36].

2.4.2 Elemental composition and chemical stability analysis

The chemical composition of the PTFE membranes was analyzed via Energy Dispersive X-ray Spectroscopy (EDS) to assess elemental distribution and structural stability. This technique operates by detecting unique X-ray spectra emitted during electron beam bombardment, enabling the precise mapping and quantification of the membrane's surface chemistry. In this study, EDS was specifically utilized to track the distribution of carbon and fluorine, providing a baseline to identify potential chemical degradation or the formation of organic deposits. By monitoring these elemental markers, the investigation aimed to confirm the chemical integrity of the PTFE matrix during exposure to the butyric acid/water azeotropic mixture [32-36].

2.4.3 Pore size and porosity analysis

The pore size distribution and surface porosity of the PTFE membranes were quantified using ImageJ software (National Institutes of Health, USA) via digital image processing of the FE-SEM micrographs. The analysis involved converting high-resolution SEM images into binary format and applying an automated thresholding algorithm to isolate individual pore areas from the polymer matrix. These segmented areas were then statistically processed to calculate the mean pore diameters and generate a comprehensive frequency distribution curve. This characterization was essential to evaluate the structural stability of the membrane and to correlate any shifts in pore morphology with the Liquid Entry Pressure (LEP) during long-term AGMD operation [37-39].

3. Results and discussion

In AGMD, the air gap width is treated as a critical baseline variable because it represents the primary source of mass transfer resistance within the system. While temperatures and flow rates control the driving force and turbulence, the air gap is the physical barrier that water vapour must diffuse through to reach the condensing surface. By keeping all other parameters constant, researchers can isolate the specific impact of this stagnant air layer on the transmembrane flux. As the gap width increases, the diffusion path length grows, which significantly lowers the flux according to Fick's law. Conversely, a wider air gap acts as a superior thermal insulator, reducing conductive heat loss from the feed to the coolant and improving the system's thermal efficiency. Establishing this baseline identifies an optimal thickness where the benefits of high permeate flux (narrow gap) and high thermal efficiency (wide gap) are effectively equilibrated. Furthermore, focusing on the gap width helps validate mathematical models regarding the transition from

ordinary diffusion to Knudsen diffusion. Without holding other variables steady, it would be impossible to distinguish whether a change in performance was due to boundary layer effects at the membrane or the physical resistance of the air gap itself.

Several experiments were conducted to separate the butyric acid/water azeotrope. The effect of various process parameters on total permeate flux (N_{Total}), selectivity of butyric acid $(\alpha_{BA})_P$, butyric acid concentration in the permeate $(C_{BA})_{Per,}$ and retentate $(C_{BA})_{Ret}$ is discussed below:

3.1 Effect of feed temperature

Figs. 3, 4 show the effect of temperature on the vapour pressure and diffusivity of water and butyric acid, as calculated by the Antoine equation Eq. (1) and the kinetic theory of gases Eq. (2), respectively. Fig. 5(a) depicts the effect of temperature of feed solution (T^B) on combined permeate flux for thickness of several air gap (AG^W), holding all other factors constant such as flow rate of feed solution (F^R) 4 l/min, temperature of coolant (CW^T) 4 °C, and flow rate of coolant (CW^R) 4 l/min. It was noted that for butyric acid/water azeotropic feed concentration, on increasing temperature of feed solution from 40 °C to 80 °C, flux increases exponentially from 0.54 Kg/m^2·h to 9.81 Kg/m^2·h for the width of air gap of 3 mm; similar increasing trends is observed for air gap width of 7mm and 11mm. This is primarily the result of the relation between the temperature and vapour pressure of butyric acid and water; as the inlet feed temperature rises, the total vapour pressure rises, resulting in an increase in the permeate flux. The vapour pressure is determined by the Antoine Equation as follows:

$$Log_{10}(P) = A - \frac{B}{C+T} \tag{1}$$

here, P is the vapour pressure in mmHg, and T is the temperature in °K. The following equation for estimating diffusivity (D_{AB}) has been derived from a combination of kinetic theory and corresponding state arguments [40].

$$\frac{PD_{AB}}{(P_{CA}P_{CB})^{\frac{1}{3}}(T_{CA}T_{CB})^{\frac{5}{12}}\left(\frac{1}{M_A}+\frac{1}{M_B}\right)^{\frac{1}{2}}} = a\left(\frac{T}{\sqrt{T_{CA}T_{CB}}}\right)^b \tag{2}$$

For pair consisting of water and non-polar gas [40]

$a = 3.640\ X\ (10)^{-4},\ \ b = 2.334$ where, D_{AB} is the diffusivity of component A in B in m/s, P is the total pressure in mmHg, M_A and M_B are the molecular weight of component A and B in kg/kmol, P_{CA} and P_{CB} are the critical pressure of component A and B in mmHg, T_{CA} and T_{CB} are the critical temperature of component A and B in °K

The selectivity of any component in MD determines its degree of separation. The term "selectivity" refers to

$$\alpha_{BA} = \left[\frac{\left(\frac{y_{BA}}{1-y_{BA}}\right)}{\left(\frac{x_{BA}}{1-x_{BA}}\right)}\right] \tag{3}$$

Here, y_{BA} and x_{BA} are the permeate butyric acid mole fraction and retentate butyric acid mole fraction.

Fig. 5(b) represents the variation in butyric acid selectivity on different temperatures of feed solution for several thickness of air gap. Fig. 5(b) shows that on increasing temperature of feed

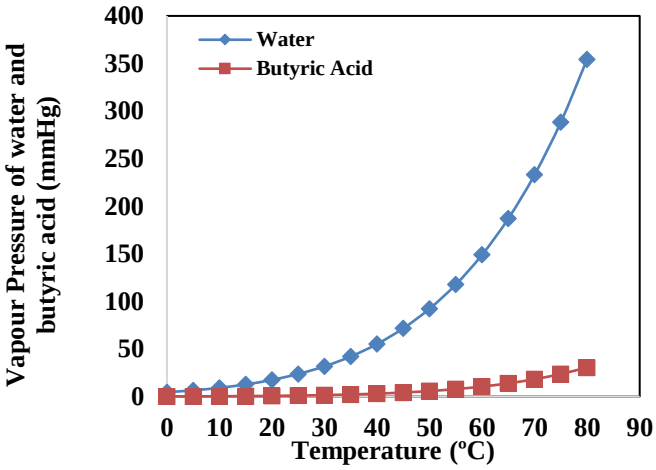

Figure 3. Effect of temperature of feed solution on vapour pressure of water and butyric acid (computed by Antoine equation

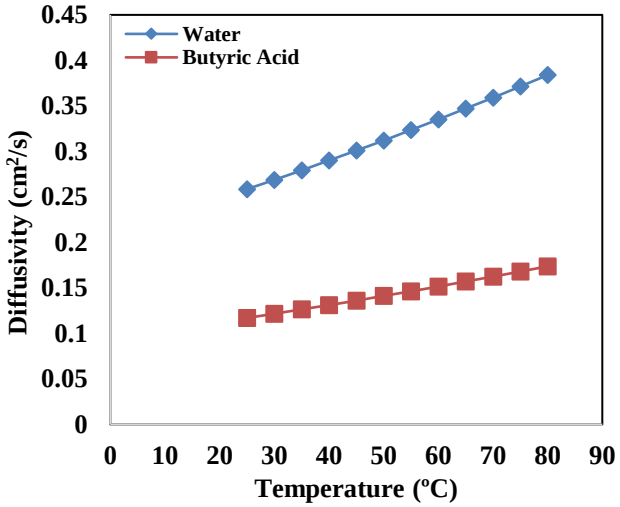

Figure 4. Diffusivity of water and butyric acid in air versus temperature computed by kinetic theory of gases

solution from 40 °C to 80 °C, the selectivity of the butyric acid decreases from 0.49 to 0.37 for width of air gap of 3mm. For air gap width of 7mm and 11mm, the similar decreasing trends is observed. It can be observed that the membrane selectivity of butyric acid in permeate was found lower than unity, which shows that a higher concentration of butyric acid is obtained in retentate as compared to permeate. Also, it can be observed from Fig. 5(c, d) that the concentration of butyric acid in permeate decreases from 10.13 weight % to 8.45 weight % while the concentration of butyric acid in retentate increases from 18.48 weight % to 19.83 weight % for air gap width of 3mm with increase in bulk feed temperature; similar results are observed for air gap widths of 7mm and 11mm. This is mainly due to less selectivity of the membrane to butyric acid vapours. The resistance to mass transfer increases with increasing air gap width; consequently, at large air gap thickness, the influence of temperature of feed solution on permeate flux is less noticeable

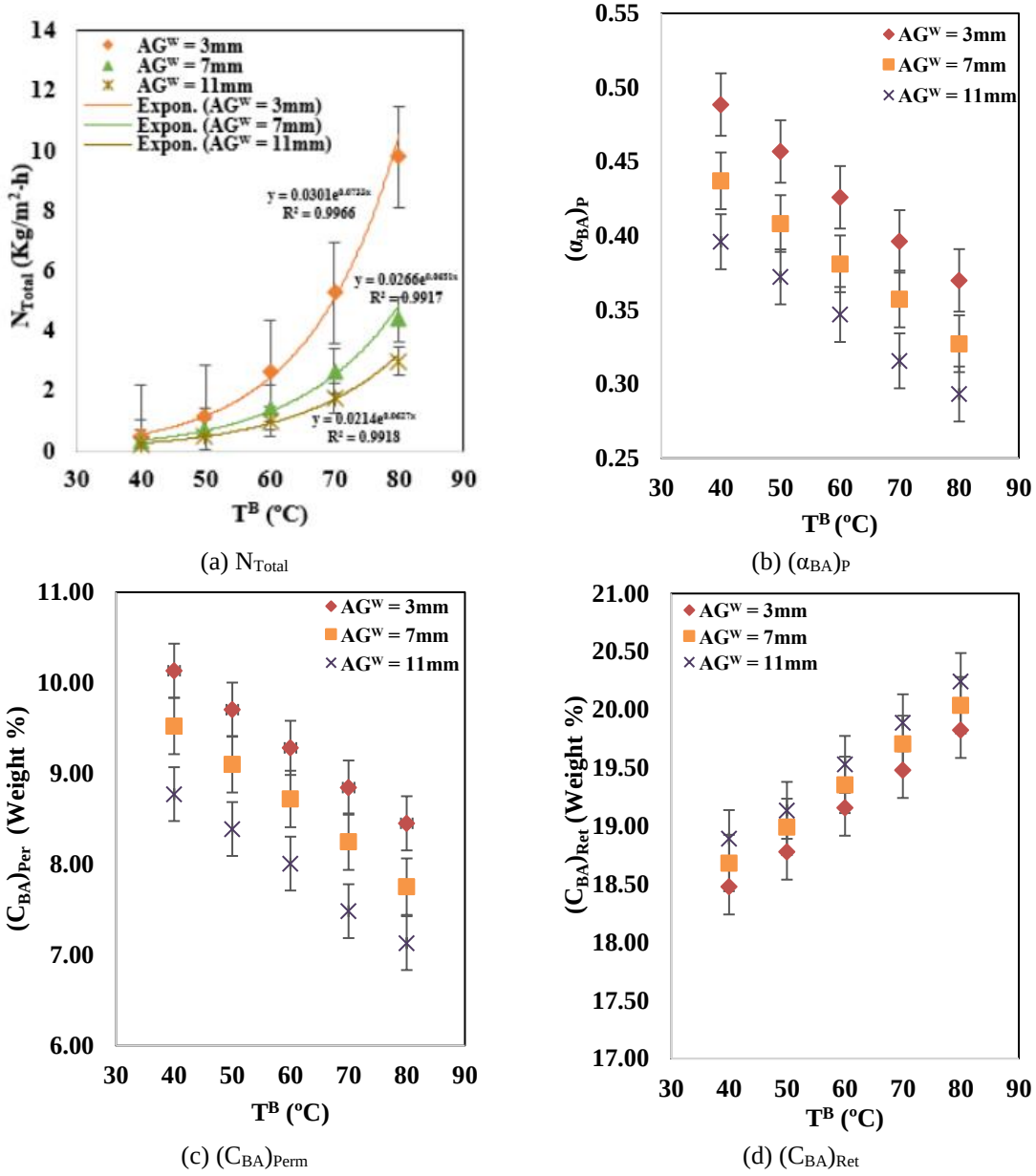

(a) N_{Total} (b) $(\alpha_{BA})_P$

(c) $(C_{BA})_{Perm}$ (d) $(C_{BA})_{Ret}$

Figure 5. Effect of temperature of feed solution at various air gap width (F^R = 4 l/min, CW^R = 4 l/min, CW^T = 4 °C)

than at small air gap thickness. Kalla et al. [41] predicted a similar behavior between feed temperature and permeate flux.

3.2 Effect of feed flow rate

Fig. 6(a, b) illustrate the influence of flow rate of feed solution on flux and selectivity of

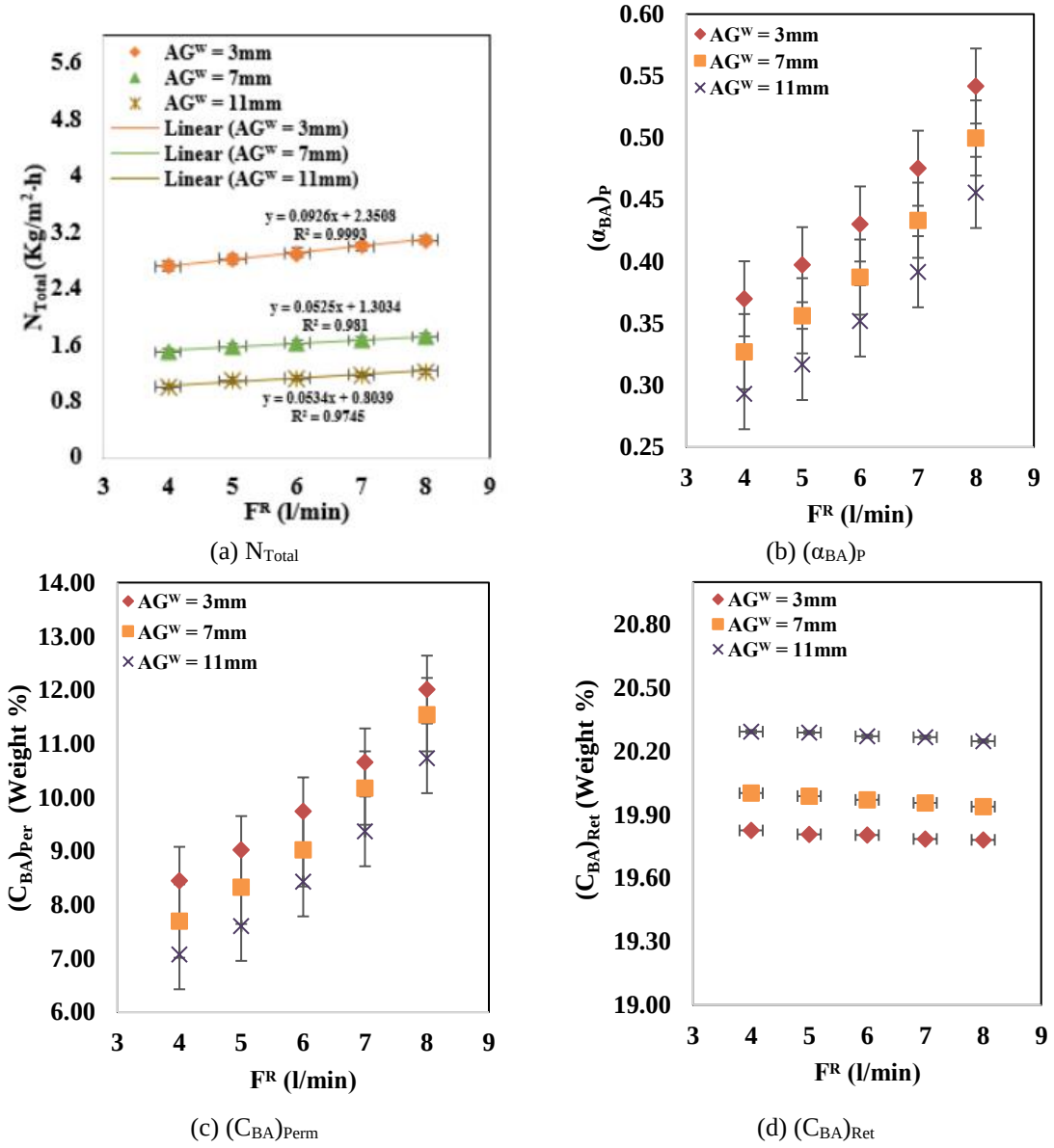

(a) N_{Total} (b) $(\alpha_{BA})_P$

(c) $(C_{BA})_{Perm}$ (d) $(C_{BA})_{Ret}$

Figure 6. Effect of flow rate of feed solution at different width of air gap (T^B = 60 ºC, CW^R = 4 l/min, CW^T = 4 ºC)

butyric acid for various distance of air gap, with all other parameters held constant, including feed inlet temperature of 60 ºC, flow rate of coolant of 4 l/min, and temperature of coolant of 4 ºC. The flux and selectivity of butyric acid in permeate increase from 2.72 Kg/m²·h to 3.09 Kg/m²·h and from 0.37 to 0.54, respectively, with a 3 mm air gap width and 4 l/min to 8 l/min increase in flow rate of feed solution. This behavior is primarily a result of the thermal boundary layer contraction caused by an increase in Reynolds number. Reynold number increases as air gap distance decreases; at 3 mm air gap thickness, Reynold number reaches its optimum. The high Reynolds

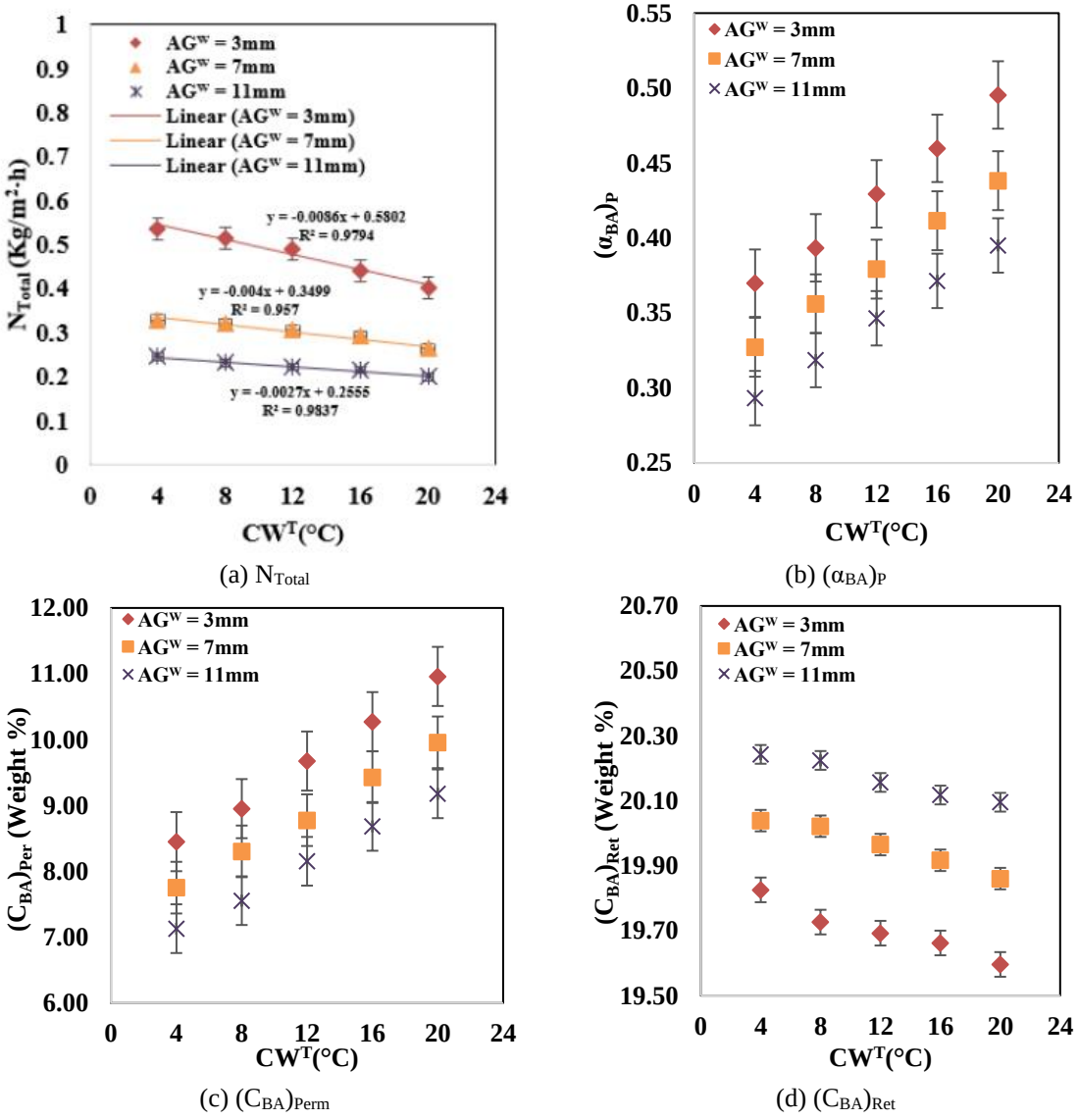

(a) N_{Total} (b) $(\alpha_{BA})_P$

(c) $(C_{BA})_{Perm}$ (d) $(C_{BA})_{Ret}$

Figure 7. Effect of temperature of coolant at different air gap thickness (T^B = 40 °C, F^R = 4 l/min, CW^R = 4 l/min)

number generates turbulence, which decreases the diffusion resistance of butyric acid vapours pass through the pores of the membrane by declining the interfacial concentration of butyric acid. At minimal width of air gap, the flow rate of feed solution significantly impacts on the permeate flux, but as air gap width increases, the feed flow rate has a much smaller impact.

3.3 Effect of coolant temperature

Fig. 7(a, b) depict the effect of temperature of coolant on the total flux and selectivity of butyric

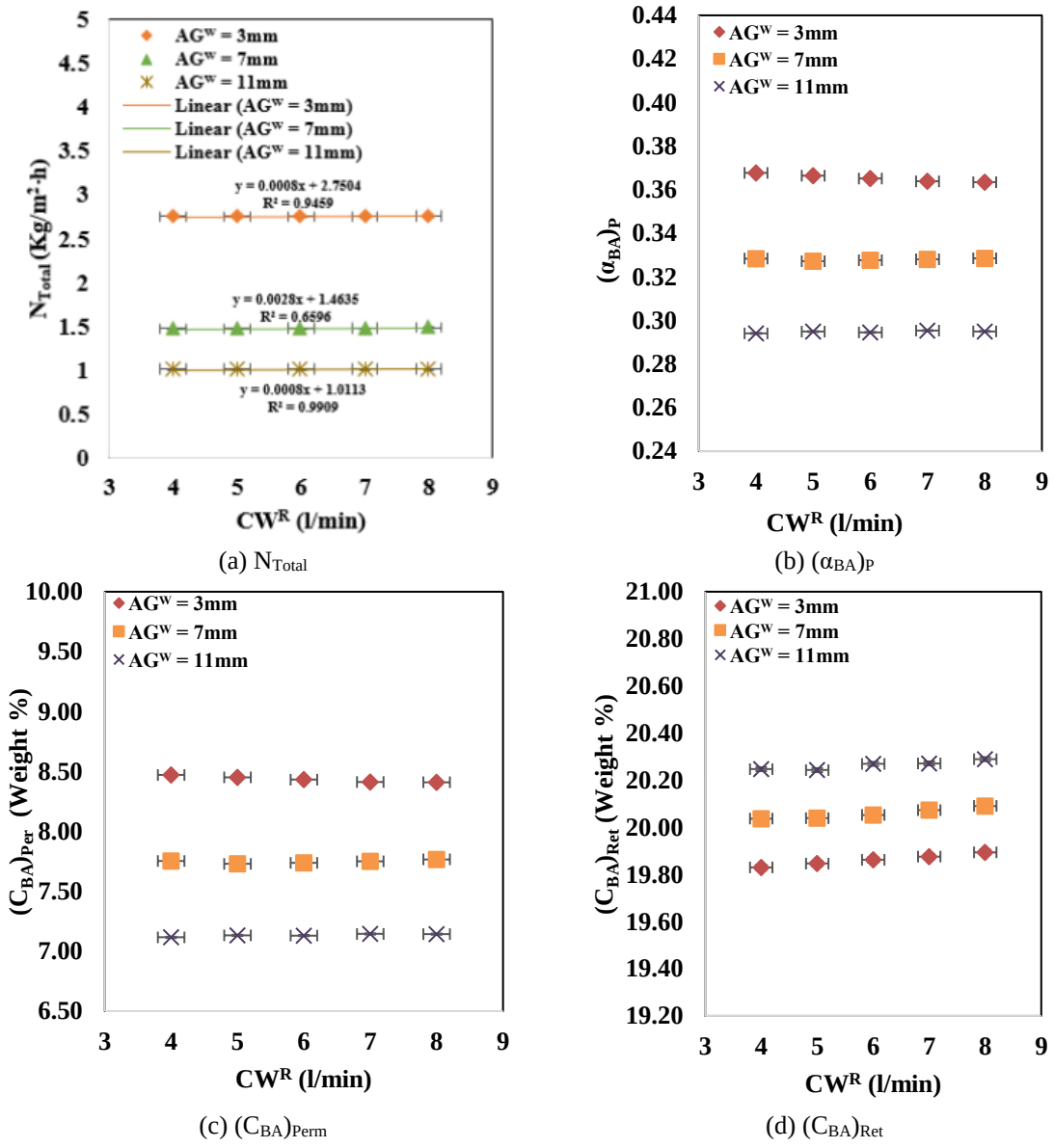

(a) N_{Total} (b) $(\alpha_{BA})_P$

(c) $(C_{BA})_{Perm}$ (d) $(C_{BA})_{Ret}$

Figure 8. Effect of flow rate of coolant at different air gap width (T^B = 60 °C, F^R = 4 l/min, CW^R = 4 °C)

acid for various thickness of air gap. It can be cleared that, on increasing the temperature of coolant from 4 °C to 20 °C, the flux decreases from 0.54 Kg/m^2·h to 0.40 Kg/m^2·h for thickness of air gap of 3 mm. This is due to a decrease in the temperature gradient across the hydrophobic microporous membrane, which reduces the vapour pressure. An increase in temperature of coolant increases the selectivity of butyric acid in permeate from 0.37 to 0.50 for air gap thickness of 3 mm. Banat et al. [25] and Kalla et al. [23] reached a similar conclusion regarding the selectivity of the HCOOH-water azeotrope and the hydrochloric acid-water azeotrope, respectively. Fig. 7(c, d) depict the variation in butyric acid concentration in permeate and retentate with temperature of

coolant. It was noted that the concentration of butyric acid increases from 8.45 weight % to 10.96 weight % in the permeate and decreases from 19.83 weight %to 19.60 weight % in the retentate for air gap width of 3 mm. Similar trends are observed for width of air gap of 7 mm and 11 mm.

3.4 Effect of coolant flow rate

The effect of flow rate of coolant on total flux and selectivity of butyric acid was examined by changing the flow rate of coolant from 4 l/min to 8 l/min, temperature of feed solution 60 °C, temperature of coolant 4 °C, and flow rate of feed solution 4 l/min. As depicted in Fig. 8(a, b), it was determined that increasing the flow rate of coolant from 4 l/min to 8 l/min did not significantly affect the total flux and selectivity of butyric acid. On increasing the flow rate of coolant from 4 l/min to 8 l/min, the total flux and selectivity of butyric acid remained nearly constant at 2.75 kg/m^2·h and 0.37 for a 3 mm air gap. This behavior is due to the fact that heat transfer coefficient (HTC) of air gap is much smaller than the HTC of heated feed side and HTC of cooling side, dominates the overall HTC. A further reason is the short length of the module, which maintains the temperature of coolant at the entrance and exit are nearly constant.

A very little variation in permeate butyric acid concentration and a significant variation in retentate butyric acid concentration was observed with changing flow rate of coolant, as indicates in Fig. 8(c, d). Due to the minor effect of the flow rate of coolant on total flux and selectivity of butyric acid, very little research has been conducted in this area [25].

3.5 Effect of air gap width

At azeotropic concentration of feed solution of butyric acid/water (18.4 weight % of butyric acid), distance of the air gap increased for different flow rates of feed solution at inlet temperature of feed solution 60 °C, flow rate of coolant 4 l/min, temperature of coolant 4 °C. As shown in Fig. 9(a, b), the total flux as well as selectivity of butyric acid decreases from 2.75 Kg/m^2·h to 1.01 Kg/m^2·h and from 0.54 to 0.46, respectively, with increasing thickness of air gap from 3 mm to 11mm, for 4 l/min flow rate of feed solution. This is because of the increase in resistances for mass transfer due to increase in width of air gap. The major disadvantage of DCMD is loss of heat due to conduction, which can be reduced by using adjustable thickness of air gap in the permeate side, which modulates the resistance of heat transfer in between the membrane and condensing plate; thus, for optimal results, the optimal air gap value must be selected.

As shown in Fig. 9, the selectivity of butyric acid and the width of the air gap varies inversely. Udriot et al. [21], Banat et al. [24], Kalla et al. [23] observed identical separation behavior for HCOOH-water and hydrochloric acid-water azeotropic mixtures, respectively. As shown in Fig. 9 (c) and 9 (d), because selectivity of butyric acid decreases as width of air gap increases, the butyric acid concentrations in the permeate and retentate inversely change with thickness of air gap. The butyric acid concentration in permeate decreases from 8.45 weight % to 7.08 weight%, while in retentate it increases from 19.83 weight % to 20.29 weight% on increasing width of air gap width from 3 mm to 11 mm at 4 l/min flow rate of feed solution.

4. Effect of operating time on Permeate flux

In a continuous AGMD operation, an azeotropic butyric acid/water solution was used as the

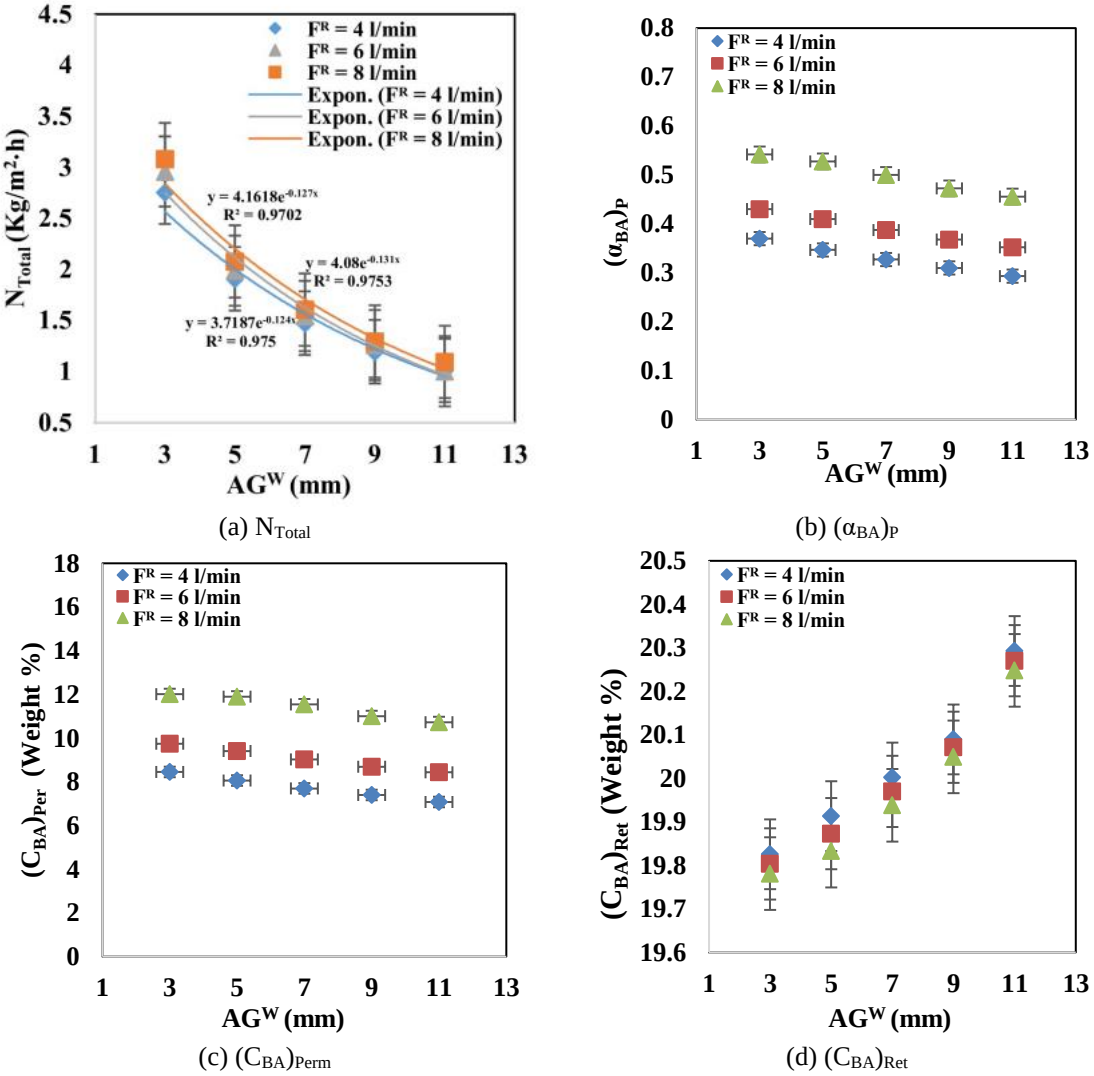

Figure 9. Effect of width of air gap at different flow rates (T^B = 60 °C, CW^R = 4 l/min, CW^T = 4 °C)

feed. As illustrated in Fig. 10, the total permeate flux was monitored over 390 hours, during which it exhibited a notable decline. At feed temperature of 80 °C, the initial flux was measured at 9.80 kg/m^2·h and remained stable for the first 110 hours, indicating an initial period of negligible fouling and steady-state operation. Subsequently, the flux declined from 9.79 to 5.55 kg/m²·h due to the gradual accumulation of organic and inorganic deposits on the surface. This run was conducted with a feed flow rate of 4 l/min, a coolant temperature of 4 °C, a coolant flow rate of 4 l/min, and an air gap width of 3 mm. Over the total duration, the flux decreased by 43.37 %, likely due to the deposition of organic and inorganic components on the hydrophobic membrane surface. This foulant layer increases mass transfer resistance without causing complete membrane failure. This fouling reduces the effective membrane parameter ($\varepsilon/\tau\delta$), thereby leading to the observed

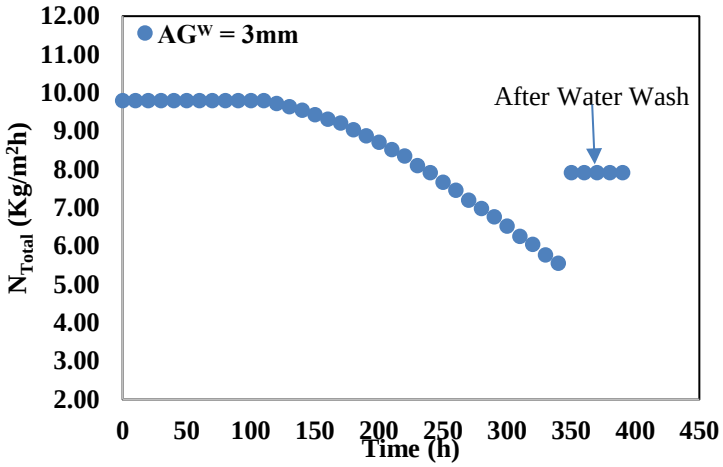

Figure 10. Change of permeate flux with operating time

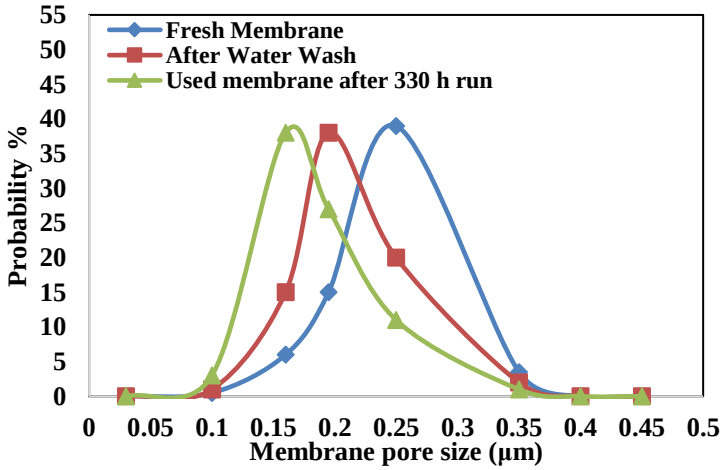

Figure 11. Pore size distribution of fresh, used and water wash PTFE membrane

reduction in total permeate flux. The similar trends were reported Kalla et al. [23], Upadhyaya et al. [44]. Since the PTFE membrane used in this study was hydrophobic and microporous in nature. it was assumed that no membrane wetting occurred. After 330 h of operation, fouling was observed on the membrane surface. Therefore, subsequent water cleaning was carried out and the membrane's effectiveness was re-evaluated. The results indicated that the total flux recovered to 7.92 kg/m^{2}h under the same process parameters, confirming the effectiveness of the cleaning process.

5. Membrane fouling study

Field Emission Scanning Electron Microscopy (FE-SEM) was utilised to examine the morphology of new, used, and washed membranes within the AGMD process. After 330 hours of

Table 4. Quantitative analysis of EDS spectra (weight % and atomic %)

Elements	Fresh Membrane		Used Membrane		Used Membrane after Water wash	
	Weight %	Atomic %	Weight %	Atomic %	Weight %	Atomic %
C	33.19	57.81	95.89	99.57	63.60	73.62
F	35.28	38.84	-	-	12.93	9.46
Au	31.53	3.35	2.66	0.17	-	-
Nb	-	-	1.15	0.15	-	-
Cl	-	-	0.30	0.11	4.61	1.81
Mg	-	-	-	-	0.39	0.22
Na	-	-	-	-	0.35	0.21
O	-	-	-	-	15.70	13.64
Al	-	-	-	-	0.29	0.15
Si	-	-	-	-	1.04	0.51
Ca	-	-	-	-	1.11	0.39
Total	100	100	100	100	100	100

experimental run of butyric acid/water azeotropic feed mixture, the membrane morphology was examined before and after water washed with bulk inlet temperature of feed solution 80 °C, flow rate of feed solution 4 l/min, temperature of coolant 4 ºC, flow rate of coolant 4 l/min, and width of air gap 3 mm. After the 330 h operation, the membrane surface exhibited organic and inorganic contamination. Upadhyaya et al. [44] and Kalla et al. [23] examined the membrane morphology in VMD and AGMD, respectively. Furthermore, Energy Dispersive Spectroscopy (EDS) confirmed the presence of carbon, and fluorine, the primary constituents of the hydrophobic PTFE membrane.

Fig. 11 displays the pore size distribution (PSD) of new, used, and water-washed PTFE membranes, as estimated via ImageJ software using SEM image data. The figure shows a clear shift toward smaller pore diameters due to fouling after a 330 h run. The Fresh Membrane peaks at 0.25 μm, but after use, the pore size reduces to 0.16 μm, indicating significant narrowing of the flow channels. The after water wash curve reveals a partial recovery to 0.20 μm, suggesting that some surface foulants were removed, internal fouling in the pore remain. This shift from 0.25 μm to 0.16 μm represents a 36% reduction, indicating that a thick layer of foulant has coated the internal walls of the pores. Figs. 12(a-c) illustrate the SEM images and EDS spectra for the fresh, used, and water washed membrane, respectively.

The Table 4 presents an elemental analysis (in weight % and atomic %) of a membrane at three different stages: fresh, used, and after a water wash. The fresh membrane shows fluorine (35.28 weight %) and carbon (33.19 w weight %t%), which is consistent with the chemical structure of PTFE. The presence of gold (Au) is likely due to the sputter coating required for SEM/EDS imaging rather than the membrane material itself. Data from the used membrane indicates that the fluorine signal drops to 0%, suggesting that the foulant layer is thick enough to completely mask the underlying PTFE substrate from the electron beam. Carbon jumps to 95.89 weight %. This suggests an accumulation of organic matter on the surface.

The water wash data indicates a fluorine reappears at 12.93 weight %, and carbon drops to

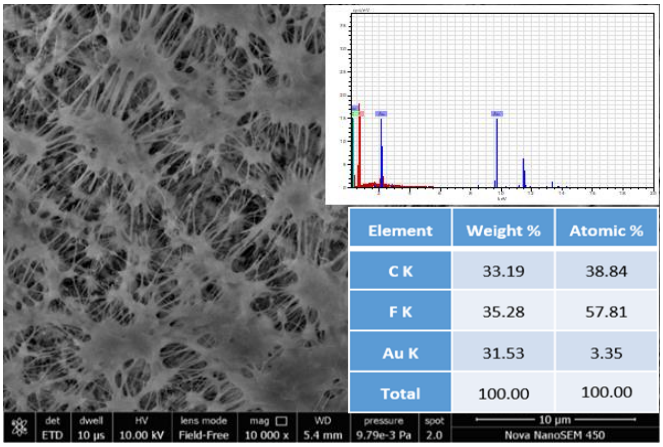

(a)

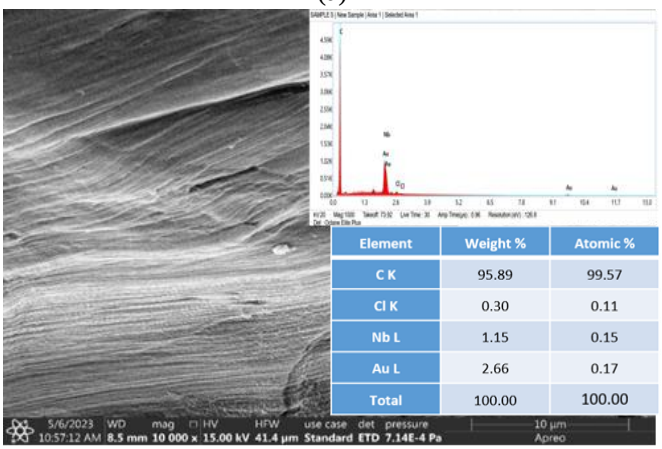

(b)

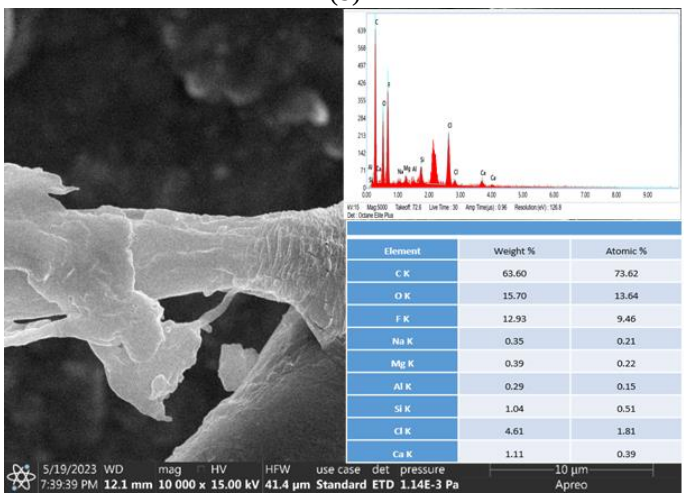

(c)

Figure 12. FESEM and EDS image of PTFE at 10,000 × magnification of a) fresh membrane b) used membrane and c) used membrane after water wash

63.60 weight %. This shows that the water wash successfully removed the top layer of foulants, allowing the EDS beam to reach the PTFE surface again. However, this stage shows a significant increase in oxygen (15.70 weight %) and various minerals like Ca, Mg, Na, and Si. The water wash removed the loose organic layer, but it failed to remove a persistent layer of inorganic scale and oxides that are more strongly adhered to the membrane pores or surface. Ultimately, EDS analysis showed a significant deposition of organic and inorganic components after 330 hours of operation.

6. Conclusions

In this study, several series of experiments were conducted to break the butyric acid - water azeotrope. The investigation focused on the effects of key operating variables, including the inlet temperature and flow rate of the feed solution, the temperature and flow rate of the coolant, and the air gap width on the total flux, butyric acid selectivity, and the concentration of butyric acid in both the permeate and retentate. Additionally, membrane morphology was analyzed to assess its performance in breaking the azeotrope. Based on the experimental findings, the following inferences can be drawn:

• Feed temperature was identified as the primary driver for mass transfer. At a 3 mm air gap, the total flux increased significantly from 0.54 kg/m²·hr to 9.81 kg/m²·hr as the feed solution temperature rose from 40 °C to 80 °C. Conversely, the selectivity of butyric acid decreased from 0.49 to 0.37 during this interval.

• As the feed solution flow rate increased from 4 to 8 l/min (at a 3 mm air gap), the total flux rose from 2.72 kg/m²·hr to 3.09 kg/m²·hr, and butyric acid selectivity increased from 0.37 to 0.54. This suggests a notable reduction in both temperature and concentration polarization.

• Coolant temperature exhibited an inverse relationship with flux but a positive correlation with selectivity. When the coolant temperature was raised from 4 °C to 20 °C at a 3 mm air gap, the permeate flux decreased from 0.54 kg/m²·hr to 0.40 kg/m²·hr, while the selectivity of butyric acid increased from 0.37 to 0.50. Increasing the coolant temperature reduces the temperature gradient across the air gap, which decreases the driving force for mass transfer while simultaneously reducing the vapor pressure of water relative to butyric acid, thereby enhancing selectivity.

• In contrast, variations in the coolant flow rate had a negligible impact on both permeate flux and solute concentration across all tested air gap widths. Increasing the coolant flow rate from 4 l/min to 8 l/min at a 3 mm air gap resulted in no observable effect on either the total flux or the selectivity of butyric acid.

• The total flux decreased from 2.75 kg/m²·hr to 1.01 kg/m²·hr when the air gap width was increased from 3 mm to 11 mm (at a feed inlet temperature of 60 °C). Simultaneously, the selectivity of butyric acid decreased from 0.54 to 0.46.

• The AGMD process effectively shifted the azeotropic composition. Butyric acid concentration in the permeate decreased as feed temperatures (40 °C to 80 °C) and air gap widths (3 to 11 mm) increased; however, it increased in the retentate. Higher feed flow rates and coolant temperatures favoured higher butyric acid concentrations in the permeate stream.

• The concentration of butyric acid in both the permeate and retentate remained nearly constant as the coolant flow rate increased from 4 l/min to 8 l/min across the 3 mm, 7 mm, and 11 mm air gaps.

• Comprehensive characterization via FE-SEM, EDS, and pore size distribution analysis

confirmed the exceptional robust nature of the PTFE membrane. After an extensive 330-hour operational period, negligible deposition or chemical degradation was observed. The stable carbon-to-fluorine ratio and maintained pore morphology confirm that the membrane's Liquid Entry Pressure (LEP) remained sufficient to prevent wetting.

• The study identifies that optimal performance for breaking the butyric acid–water azeotrope is achieved with a minimum air gap distance, elevated feed temperatures, and relatively low coolant temperatures. These findings provide a vital benchmark for scaling up AGMD processes to recover volatile organic acids from aqueous streams.

References

1. Kimura, S., Nakao, S.I., Shimatani, S.I. (1987). Transport phenomena in membrane distillation. Journal of Membrane Science, 33(2), 285-298. https://doi.org/10.1016/S0376-7388(00)80286-0
2. Yeh, G.C., Yeh, B.V., Ratigan, B.J., Correnti, S.J., Yeh, M.S., Pitakowski, D.W., Schmidt, S.T., McCarthy, A.M., Celenza, W.J. (Year). Separation of liquid mixtures by capillary distillation. Desalination, 81(1-3), 129-160. https://doi.org/10.1016/0011-9164(91)85051-U
3. Yeh, G.C., Yeh, B.V., Schmidt, S.T., Yeh, M.S., McCarthy, A.M., Celenza, W.J. (1991). Vapor-liquid equilibrium in capillary distillation. Desalination, 81(1-3), 161-187. https://doi.org/10.1016/0011-9164(91)85052-V
4. Mujiburohman, M., Sediawan, W.B., Sulistyo, H. (2006). A preliminary study: Distillation of isopropanol-water mixture using fixed adsorptive distillation method. Separation and Purification Technology, 48(1), 85-92. https://doi.org/10.1016/j.seppur.2005.07.025
5. Achari, D., Rachipudi, P., Naik, S., Karuppannan, R., Kariduraganavar, M. (2019). Polyelectrolyte complex membranes made of chitosan—PSSAMA for pervaporation separation of industrially important azeotropic mixtures. Journal of Industrial and Engineering Chemistry, 78, 383-395. https://doi.org/10.1016/j.jiec.2019.05.031
6. Banjerdteerakul, K., Peng, H., Li, K. (2023). Covalent organic frameworks based membranes for separation of azeotropic solvent mixtures by pervaporation. Journal of Membrane Science, 678, 121679. https://doi.org/10.1016/j.memsci.2023.121679
7. Castro-Muñoz, R., Msahel, A., Galiano, F., Serocki, M., Ryl, J., Hamouda, S.B., Figoli, A. (2022). Towards azeotropic MeOH-MTBE separation using pervaporation chitosan-based deep eutectic solvent membranes. Separation and Purification Technology, 281, 119979. https://doi.org/10.1016/j.seppur.2021.119979
8. Kanse, N.G., Dawande, S.D. (2017). Separation of ethanol/water (azeotropic mixture) by pervaporation using PVA membrane. Materials Today: Proceedings, 4(9), 10520-10523. https://doi.org/10.1016/j.matpr.2017.06.412
9. Fullarton, D., Schlünder, E.U. (1986). Diffusion distillation-A new separation process for azeotropic mixtures Part 1: Selectivity and transfer efficiency. Chemical Engineering and Processing: Process Intensification, 20(5), 255-263. https://doi.org/10.1016/0255-2701(86)80018-6
10. Li, X., Ye, Q., Li, J., Liu, Y., Yan, L., Jian, X., Zhang, S. (2023). Investigation on energy-efficient heterogeneous pressure-swing azeotropic distillation for recovery of cyclohexane and tert-butanol from industrial effluent. Separation and Purification Technology, 306, 122705. https://doi.org/10.1016/j.seppur.2022.122705
11. Mortaheb, H.R., Kosuge, H. (2004). Simulation and optimization of heterogeneous azeotropic distillation process with a rate-based model. Chemical Engineering and Processing: Process Intensification, 43(3), 317-326. https://doi.org/10.1016/S0255-2701(03)00131-4
12. Shan, B., Niu, C., Meng, D., Zhao, Q., Ma, Y., Wang, Y., Zhang, L. (2021). Control of the azeotropic distillation process for separation of acetonitrile and water with and without heat integration. Chemical

Engineering and Processing: Process Intensification, 165, 108451. https://doi.org/10.1016/j.cep.2021.108451
13. Zhang, H., Jiao, Y., Zhao, Q., Li, C., Cui, P., Wang, Y., Ma, Y. (2022). Sustainable separation of ternary azeotropic mixtures based on enhanced extractive distillation/pervaporation structure and multi-objective optimization. Separation and Purification Technology, 298, 121685. https://doi.org/10.1016/j.seppur.2022.121685
14. Graczová, E., Šulgan, B., Steltenpohl, P. (2020). tert-Butanol-water mixture separation by extractive distillation: Application of experimental data in process simulations. Separation and Purification Technology, 251, 116968. https://doi.org/10.1016/j.seppur.2020.116968
15. Lek-utaiwan, P., Suphanit, B., Douglas, P.L., Mongkolsiri, N. (2011). Design of extractive distillation for the separation of close-boiling mixtures: Solvent selection and column optimization. Computers & Chemical Engineering, 35(6), 1088-1100. https://doi.org/10.1016/j.compchemeng.2010.12.005
16. Li, R., Meng, X., Liu, X., Gao, J., Xu, D., Wang, Y. (2019). Separation of azeotropic mixture (2, 2, 3, 3-Tetrafluoro-1-propanol + water) by extractive distillation: Entrainers selection and vapour-liquid equilibrium measurements. The Journal of Chemical Thermodynamics, 138, 205-210. https://doi.org/10.1016/j.jct.2019.06.026
17. Varyemez, H.S., Kaymak, D.B. (2022). Effect of operating pressure on design of extractive distillation process separating DMC-MeOH azeotropic mixture. Chemical Engineering Research and Design, 177, 108-116. https://doi.org/10.1016/j.cherd.2021.10.029
18. Yang, A., Yang Kong, Z., Sunarso, J., Su, Y., Wang, Q., Zhu, S. (2022). Insights on sustainable separation of ternary azeotropic mixture tetrahydrofuran/ethyl acetate/water using hybrid vapor recompression assisted side-stream extractive distillation. Separation and Purification Technology, 290, 120884. https://doi.org/10.1016/j.seppur.2022.120884
19. Zhang, Y., Xu, X., Yang, H., Gao, J., Xu, D., Zhang, L., Wang, Y. (2020). Separation of azeotropic mixture isopropyl alcohol + ethyl acetate by extractive distillation: Vapor-liquid equilibrium measurements and interaction exploration. Fluid Phase Equilibria, 507, 112428. https://doi.org/10.1016/j.fluid.2019.112428
20. Mahdi, T., Ahmad, A., Nasef, M.M., Ripin, A. (2015). State-of-the-art technologies for separation of azeotropic mixtures. Separation & Purification Reviews, 44(4), 308-330. https://doi.org/10.1080/15422119.2014.963607
21. Udriot, H., Araque, A., von Stockar, U. (1994). Azeotropic mixtures may be broken by membrane distillation. Chemical Engineering Journal and the Biochemical Engineering Journal, 54(2), 87-93. https://doi.org/10.1016/0923-0467(93)02814-D
22. Udriot, H., Araque, A., Von Stockar, U. (1994). Azeotropic mixtures may be broken by membrane distillation. Chemical Engineering Journal, 54.
23. Kalla, S., Upadhyaya, S., Singh, K., Baghel, R. (2019). Experimental and mathematical study of air gap membrane distillation for aqueous HCl azeotropic separation. Journal of Chemical Technology & Biotechnology, 94(1), 63-78. https://doi.org/10.1002/jctb.5766
24. Kalla, S., Baghel, R., Upadhyaya, S., Singh, K. (2021). Separation of HCl/water mixture using air gap membrane distillation, Taguchi optimization and artificial neural network. Chemical Product and Process Modeling, 17(1), 17-20. https://doi.org/10.1515/cppm-2020-0078
25. Banat, F.A., Al-Rub, F.A., Jumah, R., Shannag, M. (1999). Theoretical investigation of membrane distillation role in breaking the formic acid-water azeotropic point: Comparison between Fickian and Stefan-Maxwell-based models. International Communications in Heat and Mass Transfer, 26(6), 879-888. https://doi.org/10.1016/S0735-1933(99)00076-7
26. Banat, F.A., Abu Al-Rub, F., Jumah, R., Shannag, M. (1999). On the effect of inert gases in breaking the formic acid-water azeotrope by gas-gap membrane distillation. Chemical Engineering Journal, 73(1), 37-42. https://doi.org/10.1016/S1385-8947(99)00014-5
27. Dwidar, M., Park, J.Y., Mitchell, R.J., Sang, B.I. (2012). The future of butyric acid in industry. The Scientific World Journal, 2012. https://doi.org/10.1100/2012/471417
28. Karimi, G., Vahabzadeh, M. (2014). Butyric acid. In Encyclopedia of Food Microbiology (Vol. 1, 3rd

ed.). Elsevier. https://doi.org/10.1016/B978-0-12-386454-3.00591-1
29. Ramey, D. (2004). Production of butyric acid and butanol from biomass. Biomol Engineering.
30. Xu, Z., Jiang, L. (2011). Butyric acid. Comprehensive Biotechnology 2nd ed., 3, 207-215. Elsevier. https://doi.org/10.1016/B978-0-08-088504-9.00181-1
31. Jiang, L., Fu, H., Yang, H.K., Xu, W., Wang, J., Yang, S.T. (2018). Butyric acid: Applications and recent advances in its bioproduction. Biotechnology Advances, 36(8), 2101-2117. https://doi.org/10.1016/j.biotechadv.2018.09.005
32. Sharma, A., Soti, A., Gupta, A.B. (2024). Identifying artifacts in EDS of fouled RO membranes through Raman and ICP-MS analysis. Desalination and Water Treatment, 317, 100295. https://doi.org/10.1016/j.dwt.2024.100295
33. Navarro-Tovar, R., Gorgojo, P., Jobson, M., Martin, P., Perez-Page, M. (2024). Innovations in water desalination: Enhancing air gap membrane distillation performance by the incorporation of clay nanoparticles into PVDF matrix membranes. Environmental Science: Water Research & Technology, 10(10), 2418-2431. https://doi.org/10.1039/d4ew00326h
34. Sun, J., Yan, M., Tao, G., Su, R., Xiao, X., Wu, Q., Zheng, T., Zhao, H. (2025). A single-atom manganese nanozyme mediated membrane reactor for water decontamination. Water Research, 268, 122627. https://doi.org/10.1016/j.watres.2024.122627
35. Wang, H., Cao, Y., Li, B., Shen, L., Wu, X.L., Li, R., Yang, J. (2025). Photothermal nano-confinement reactor with bimetallic sites for enhanced peroxymonosulfate activation in antibiotic degradation. Water Research, 268, 122623. https://doi.org/10.1016/j.watres.2024.122623
36. Li, Y., Ma, J., Lin, H., Chen, C., Raza, S., Zeng, Q., Zhang, Y. (2025). Unique dual superlyophobic covalent organic frameworks (COF-TpBD) intercalated MXene composite membrane for efficient oil-water separation. Journal of Membrane Science, 717, 123579. https://doi.org/10.1016/j.memsci.2024.123579
37. Gao, S.S., Zhang, X.H., Geng, M.Y., Tian, J.Y. (2025). Effect of membrane material and pore size on membrane fouling during filtration of algae-laden water. Water Science and Engineering, 18(3), 335-344. https://doi.org/10.1016/j.wse.2025.04.001
38. Bindels, M., Andrés-Mañas, J.A., Ding, W., Hitsov, I., Mutlu-Salmanli, O., Hardikar, M., Van der Bruggen, B. (2026). Pilot-scale membrane distillation modeling: Validation, comparison, and consensus. Desalination, 620, 119674. https://doi.org/10.1016/j.desal.2025.119674
39. El Mokhtar, I., Boubakri, A., Bouguecha, S.A.T., Hafiane, A. (2019). Modeling and experimental study of air gap membrane distillation unit: Application for seawater desalination. Desalination and Water Treatment, 154, 72-81. https://doi.org/10.5004/dwt.2019.23889
40. Bird, R.B., Stewart, W.E., Lightfoot, E.N. (2001). Transport phenomena (2nd ed.). John Wiley & Sons, Inc.
41. Kalla, S., Upadhyaya, S., Singh, K., Baghel, R. (2019). Development of heat and mass transfer correlations and recovery calculation for HCl-water azeotropic separation using air gap membrane distillation. Chemical Papers, 73(10), 2449-2460. https://doi.org/10.1007/s11696-019-00795-w
42. Thiruvenkatachari, R., Manickam, M., Ouk Kwon, T., Shik Moon, I., Woo Kim, J. (2006). Separation of water and nitric acid with porous hydrophobic membrane by air gap membrane distillation (AGMD). Separation Science and Technology, 41(14), 3187-3199. https://doi.org/10.1080/01496390600854651
43. Kalla, S., Upadhyaya, S., Singh, K., Baghel, R. (2019). Experimental and mathematical study of air gap membrane distillation for aqueous HCl azeotropic separation. Journal of Chemical Technology & Biotechnology, 94(1), 63-78. https://doi.org/10.1002/jctb.5766
44. Upadhyaya, S., Singh, K., Chaurasia, S.P., Dohare, R.K., Agarwal, M. (2016). Recovery and development of correlations for heat and mass transfer in vacuum membrane distillation for desalination. Desalination and Water Treatment, 57(55), 26886-26898. https://doi.org/10.1080/19443994.2016.1189245